Analytical Methods

Accepted Manuscript

This article can be cited before page numbers have been issued, to do this please use: J. Liu, X. Chen, R. Shen, S. Liu, X. Xiao, J. Yan, Y. Zhang, Z. Jiang and B. Nie, *Anal. Methods*, 2020, DOI: 10.1039/D0AY00633E.

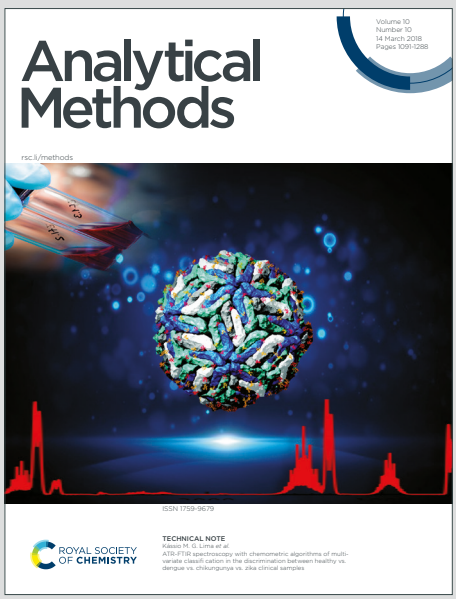

ROYAL SOCIETY OF CHEMISTRY

rsc.li/methods

View Article Online
DOI: 10.1039/D0AY00633E

ARTICLE

Sensitive detection of single-cell secreted lactic acid for glycolytic inhibitor screening with a microdroplet biosensor

Received 00th January 20xx,
Accepted 00th January 20xx

DOI: 10.1039/x0xx00000x

Xuyue Chen[a †], Rui Shen[a †], Sidi Liu[a †], Xiang Xiao[a], Jun Yan[a], Yiqiu Zhang[a], Zhongyun Jiang[a], Baoqing Nie[b], Jian Liu[a *]

Lactic acid (LA) plays an important role in the tumor metabolism and malignant progression of various cancer. Herein, we have developed a one-step, free-wash microfluidic approach with droplet biosensors for sensitive detection of LA secreted by a single tumor cell. Our assay integrates an enzyme-assisted chemical conversion of LA in the small volume (4.2 nL) droplets for fluorescent signal readout. The microdroplet assay has achieved a limit of detection (1.02 μM), more sensitive than the commercial ELISA kit by nearly two orders of magnitude. A good specificity has been demonstrated for this assay by testing various ions and biomolecules from the culture medium. This droplet assay allows us to acquire the profiles of lactic acid secretion of tumor cells under the influence of glycolytic inhibitors at the single-cell level. It offers a useful research tool to study the cell-to-cell differences of LA secretion and glycolytic inhibitor screening for cancer research.

Introduction

Tumor cells undergo abnormal metabolisms to modulate their extracellular microenvironment to be acidic, which favors the proliferation, migration, and invasion of tumor cells instead of normal cells[1-3]. The slightly acidic tumor microenvironment is contributed by lactic acid (LA) and carbonic acid, with the assistance of some pH regulatory factors such as V-ATPase[4-8]. The production of LA is associated with the glycolytic pathway[6, 7]. The generation of carbonic acid is derived from CO_2 and H_2O catalyzed by carbonic anhydrase overexpressed in tumor cells[4, 5, 9]. The accumulation of LA has been demonstrated to be crucial for tumor proliferation, metastasis, angiogenesis, immune escape, and resistance to radio/chemotherapies, far more than a metabolic waste[6, 10]. The studies of LA accumulation on tumor progression have been performed in leukemia, lymphoma, multiple myeloma, lung cancer, breast cancer, head and neck cancer[11-15]. They suggest that the clinical samples in the metastatic spread cases frequently exhibit a wider range and higher levels of lactate, in comparison to the non-metastatic tumor cases. Back to early days, Otto Warburg first reported the abnormal characteristics of cancer cell metabolism in the 1920s, suggesting lactic acid as a characteristic product of tumor cell release[16]. Usually under hypoxic conditions, normal cells can produce ATP by glycolysis as the secondary pathway for energy supply, accompanied with conversion of pyruvate (PA) to lactic acid in presence of lactate dehydrogenase (LDH) and reduced coenzyme I (NADH)[17]. In contrast, cancer cells tend to go through the glycolytic pathway even in normoxia, resulting in a large amount of lactic acid secretion responsible for acidification of the tumor microenvironment (i.e. "Warburg effect") (Scheme 1A)[16, 18]. Based on estimation of several recent studies, the secretion rate of LA in tumor cells was approximately 10^{-16} mol cell^{-1} sec^{-1}, much higher than the typical secretion rate of leukocytes or normal cells[19-21]. Nevertheless, these results were generally calculated on the average of large cell populations, without taking account of the complex heterogeneity in cancer cells.

The techniques based on single-cell analysis can provide the critical information of cell-to-cell difference in genomics[22, 23], transcriptomics[24, 25], and proteomics[26, 27]. The advances in microfluidics have provided flexible platforms for single-cell experiments in biomedical research and applications[28-30].Di Carlo et al. developed a gelatin microdroplet platform for high-throughput sorting of micro algal monoclones with high lipid productivity or biomass accumulation[31]. Microfluidic droplet biosensors were developed to detect single-cell secreted matrix metalloproteinase (MMP9) activities for evaluation of cancer cell invasiveness[32], or the extracellular hydrogen peroxide levels secreted by a single cell assisted with Au nanoclusters[33]. Scoles et al. adopted a pH-sensitive dye to monitor the acidic changes inside the individual cell-encapsulated droplets, therefore indirectly reflecting the lactate secretion at the single-cell level[20]. However, the assay of using a pH-sensitive dye was not specific to lactic acid, thus subject to interference by the generation of carbonic acid involved in cellular activities, or by mixing with any solutions which can buffer the protons.

[a] Institute of Functional Nano and Soft Materials (FUNSOM), Jiangsu Key Laboratory for Carbon-Based Functional Materials and Devices, Soochow University, Suzhou, Jiangsu Province, 215123, China.
[b] School of Electronic and Information Engineering, Soochow University, Suzhou, Jiangsu Province, 215006, China.
† These authors contributed equally to this manuscript.
* Corresponding author: Prof. Jian Liu, jliu@suda.edu.cn
iMINTS Lab, http://web.suda.edu.cn/jliu/index.html
Electronic Supplementary Information (ESI) available: [Generation of size-tunable droplets, cell density titration, optimization of the fluorescent assay, lactic acid secretion by single MCF7 or HUVEC cells in droplets, inhibitor tests]. See DOI: 10.1039/x0xx00000x

View Article Online DOI: 10.1039/D0AY00675E

Herein, we report a new assay for highly sensitive and specific detection of single-cell secreted lactic acid in the format of microdroplet biosensor (**Scheme 1**). Although lactic acid itself does not exhibit any extraordinary fluorescent property or unique UV-Vis absorbance, our microdroplet biosensor integrates the biochemical reaction of lactate dehydrogenase-assisted conversion of lactic acid, where the product of protonated nicotinamide adenine dinucleotide (NADH) becomes fluorescent (**Scheme 1B**)[34, 35]. Different from the report which employed fluorescein as an external probe for indirect measurement of lactate[36], our method does not require the additional fluorophore such as fluorescein, instead, relies on the intrinsic fluorescent change produced by lactic acid conversion. There are two key technological features in the design of our assay: (1) A one-step, label-free, and no-wash procedure to detect the fluorescent byproduct of lactic acid conversion. (2) High throughput generation (2.6 x 10^3 events/min) of microdroplets in small volume (4.2 nL/each) encapsulating single cells to study cell-to-cell difference in lactic acid secretion (**Scheme 1C**). We have demonstrated that our droplet assay is highly specific to the molecule of lactic acid, which is distinctly different from the report of using a pH-sensitive dye[20]. Compared against a commercial ELISA kit for lactic acid detection, the experiments support that our droplet assay can improve the limit of detection by nearly two orders of magnitude. It allows us to perform a pilot screening experiment to study the glycolytic inhibitors, including 3-bromopyruvic acid (3BP), Vitamin K_1 (VK_1), and Vitamin K_3 (VK_3), at the single-cell level. This droplet assay promises a new tool for the fundamental research of cell heterogeneity in cancer metabolism.

Experimental section

Materials and reagents.

Mineral oil, phorbol 12-myristate 13-acetate (PMA), ethanol, lactic acid, lactate dehydrogenase (LDH), Vitamin K_1 (VK_1) and Vitamin K_3 (VK_3) were obtained from Sigma-Aldrich. The commercial kit of lactic acid detection (cat# ml037915) was provided by Shanghai Enzyme Linked Biotechnology Co., Ltd. 4',6-diamidino-2-phenylindole (DAPI) was obtained from Dojindo Laboratories (Kumamoto, Japan). The emulsifier of ABIL EM 90 (Degussa), 1/16 Y-shaped small plastic hose nipple, and glass capillaries were obtained from the general suppliers. β-Nicotinamide adenine dinucleotide trihydrate (NAD) was acquired from Shanghai Yesen Biotechnology CO. 3-Bromopyruvic acid (3BP) was provided by Tokoyo Chemical Industry Co., Ltd. T-shaped PEEK chromatography connectors (IDEX Healthy & science, P-713) and PVC tubing (Tygon, R-3603 1/8''OD), were purchased from the suppliers as specified.

Fluorescent assay for lactic acid detection.

The fluorescent assay for lactic acid detection was verified by spectral analysis of a series of reagent combinations with a microplate reader (Varioskan flash, Thermo Scientific) and a fluorescence spectrometer (HORIBA FluoroMax 4), including (1) Tris-HCl buffer (pH=7) as the blank control; (2) LA (25 mM); (3) NAD (6 mM); (4) LDH (200 U L^{-1}); (5) NAD (6 mM) + LA (25 mM); (6) NAD (6 mM) + LDH (200 U L^{-1}); (7) LA (25 mM) + LDH (200 U L^{-1}); (8) NAD (6 mM) + LA (25 mM) + LDH (200 U L^{-1}). All the solutions were prepared in the Tris-HCL buffer, and then mixed as specified.

Assay specificity.

The specificity of the system for lactic acid detection was verified by spectral analysis of a series of reagents using a fluorescence spectrometer. The reagents in our tests included K^+, Cu^{2+}, Na^+, Mg^{2+}, Cl^-, glucose, vitamin C, glutathione, arginine, and LA. All of them were tested in the concentration of 100 mM. These ions and biomolecules were chosen as a group common species in the cell culture medium or in the body fluids of mammals. These tests would provide valuable information to evaluate the potential risk of signal interference for the subsequent experiments.

Verification of cell-secreted lactic acid with a commercial kit.

A commercial ELISA kit was employed to detect the lactic acid level secreted by cancer cells for comparison. The cell samples (6 x 10^6) were centrifuged for 20 minutes at 1000×g. After removal of the precipitation, the commercial ELISA kit was immediately performed to detect lactic acid, according to the supplier's protocol. A standard sandwich method was implemented by using horseradish peroxidase-tagged antibody and a plate coated with the capture antibody in this ELISA kit. The substrate of 3,3',5,5'-Tetramethylbenzidine (TMB) was incubated with the assay mixture, to measure the OD value by a microplate reader (Varioskan flash, Thermo Scientific).

Generation of microdroplets.

The capillary microfluidic device was assembled to generate droplets as described previously[33]. In brief, the capillary set-up was made of two PEEK chromatography T-type connectors, three glass capillaries, Y-type hose, and two pair of customized adapters. The injected continuous phase was mineral oil containing surfactant, ABIL EM 90(2 wt. %), which flowed into the gap of the double pipe-like structure. The dispersed phase was cell suspension and a Tris-HCl mixture of LDH and NAD. The liquid was delivered by using the syringe pumps (LSP02-1B, the flow rate coefficient of variation < 0.5%, Longer Precision Pump Co., Ltd.). The two aqueous phases were merged through the Y-type hose. Once the dispersed and continuous phase contacted each other in the narrow gap region defined by the capillary orifices, the water-in-oil microdroplets were generated in a high throughput format, and collected into a confocal dish. The size of microdroplets was tunable by changing the narrow gap between the orifices, or controlling the flow rate ratio of the two liquid phases. A typical droplet diameter (200 μm) was achieved with 5 μL min^{-1} for the continuous phase and 20 μL min^{-1} for the dispersed phase. The process of microdroplet generation was monitored by a stereo microscope (SZ680) mounted with a high-speed video recorder (MDX4-T). The size distribution was determined by measuring the diameters of the droplets (n=308) in bright-field images, acquired with an Olympus IX71 microscope (objective 10×, Olympus, USA) and analyzed by the software of Nano measurer (Fudan University, China).

Cell culture.

View Article Online
DOI: 10.1039/D0AY00637F

Human Umbilical Vein Endothelial Cells (HUVEC), human breast cancer cells (MCF7), and human non-small cell lung cancer cells (A549) were obtained from American type culture collection (ATCC). They were cultured in DMEM medium (Gibco, USA) supplemented with heat-inactivated 10% (v/v) fetal bovine serum (FBS, Invitrogen, Carlsbad, CA), 100 U mL^{-1} penicillin, 100 µg mL^{-1} of streptomycin and Glutamine at 37°C under humidified atmosphere with 5% CO_2.

Encapsulating single cells in microdroplets.

The cell sample were trypsinized, centrifuged, washed once with PBS buffer (pH 7.4), and then resuspended in Phenol Red-free DMEM culture medium. The concentration of the cell suspension was determined by direct counting using a standard bright line hemocytometer (Sigma-Aldrich).

Different cell loading concentrations (6 x 10^4, 6 x 10^5, and 6 x 10^6 cells mL^{-1}) were tested to titrate the number of cells encapsulated by the droplets. The cell nuclei were stained with DAPI dye for 15 minutes. Image stacks of the cell-wrapped droplets were acquired by z-axis scanning with a confocal laser scanning microscope (Zeiss LSM 800). One image stack was composed of 10 continuously sectioned images which were automatically acquired with a step interval of 20 µm, thus covering a z-axis depth of 200 µm. In each cell loading density, 6 image stacks (60 sectioned images) as the randomly-chosen areas of interest were analyzed for cell counting. There were approximately one hundred droplets in total in 6 image stacks under comprehensive three-dimensional imaging analysis. Detailed experimental procedures and cell counting inside the droplets are available in the supplementary information.

Detection of lactic acid secreted by single cells encapsulated in the microdroplets.

The lactic acid secretion was detected at the single cell level after the cells were encapsulated into the droplets. The cell suspension and the reaction solution were separately loaded in two sterile medical syringes, and mixed quickly at the Y-type hose. Uniform microdroplets containing the mixture were formed at the capillary orifices, and collected in the confocal dishes at room temperature in an air-conditioned room. Due to the isolation of water-in-oil emulsion, the influence by the other environmental factors such as humidity on cell secretion inside the droplets was reduced to a minimal level. The reaction solution was composed of NAD (6 mM), LDH (200 U L^{-1}). It was pre-mixed with or without additive chemical compounds[37, 38], such as PMA (56 µM), 3BP (3 µM), VK_1 (23.5 µM) or VK_3 (23.5 µM), depending on the individual experiments as specified elsewhere. Given the fact that the IC_{50} values of the enzyme inhibitors were generally reported on the use of large cell populations with traditional techniques (note: IC_{50} for VK1 not available)[39-41], the inhibitor doses tested in our droplet experiments were lower than their IC_{50} values for the requirement of single-cell experiments. The fluorescence of the microdroplets were monitored at the elsewhere specified time points with an inverted fluorescence microscope (Olympus IX71, objective 10x) equipped with a multispectral imaging CCD camera (Nuance, CRI). The fluorescent images were acquired at the channel of excitation/emission (360 nm/490 nm). In order to calibrate the fluorescence change to lactic acid concentration, a gradient series of lactic acid solutions were encapsulated into droplets under the identical conditions for quantitative analysis.

Imaging analysis.

Deconvolution of the fluorescence image cubes acquired by the Nuance CCD camera were performed by referring to a standard spectral library of NADH fluorescence and the background noise baseline of the negative controls. The fluorescent intensities of microdroplets at the NADH channel were analyzed with the built-in software of the Nuance camera, according to an intensity threshold-dependent segmentation method. The fluorescence intensity (f_{avg}) on the average for each experimental condition was defined as the sum of the calculated intensity-weighted pixel area divided by the sum of the pixel area for each droplet, as illustrated by the equation (1).

$$f_{avg} = \frac{\sum_1^n f_n p_n}{\sum_1^n p_n}$$

where f_n is the fluorescence intensity of each pixel, p_n is the pixel area in the segmented droplet, and n is the number of the microdroplets counted for each test. Generally, multiple area of interest (AOI) were identified and analyzed for each sample/test. Typically, each AOI contained 14-20 individual droplets. Each droplet covered $12.8 \pm 1.4 \times 10^3$ pixels. In each testing condition, we randomly chose 3 separate AOIs as the image cubes (n=3) for fluorescent quantification. The data were exported to the Origin v.8.0 (OriginLab, Northampton, MA, USA) for further statistical processing.

Results and discussion

Generation of diameter-adjustable microdroplets encapsulating single cells.

Microdroplets of water-in-oil emulsions were generated via the home-made capillary device after loading the liquids of the continuous phase (mineral oil containing 2 wt% ABIL EM 90) and the dispersed phase (cell suspension and aqueous solution of the reagent mixture). When the two immiscible phases flew into the narrow gap defined by the capillary orifices, their flow streams were altered to produce water-in-oil microdroplets (Scheme 1). The flow rate ratio of the two liquid phases was adjustable for tuning the diameter of the droplets (Fig. S1A). The process of droplet generation with diameter-tuning was monitored using a high-speed video recorder, as shown in the snapshot micrographs of video clips (Fig. S1B). In Fig. S1C, in the case of a fixed dispersed phase flow rate (Q_d) of 5 µL min^{-1}, a series of flow rates of continuous phase (Q_c), including 10, 15, 20, 25, 30, 40, 50 µL min^{-1}, were tested to produce microdroplets of different diameters. With the increase of the flow rate ratio (Q_d / Q_c) from 1 to 10, the diameter of droplets was gradually enlarged from 110 to 400 nm (Fig. S1A and Fig. S1C)[33]. The droplet size was uniform under each flow condition, indicating a highly reproducible performance with our device. For instance, the size distribution of the droplets from 7 different batches at the fixed flow rates (Q_c: 20 µL min^{-1}; Q_d: 5

View Article Online DOI: 10.1039/D0AY00637F

µL min^{-1}) was statistically analyzed and present in Fig. S2. The throughput of droplet production was approximately 2.6 x 10^3 droplets per minute.

In the case of the fixed flow rates (the dispersed phase Q_d: 5 µL min^{-1}; the continuous phase Q_c: 20 µL min^{-1}), the cell solutions in different concentrations (6 x 10^4, 6 x 10^5 and 6 x 10^6 cells mL^{-1}) were loaded into the device to study the cell encapsulation profiles in individual microdroplets. The cell nuclei were pre-stained with DAPI dye for the purpose of easier identification inside the microdroplets. The cells encapsulated by the droplets were enumerated by image analysis with confocal laser scanning microscopy (Zeiss LSM 800) in the Z-axis scanning mode (Fig. S3). When the cell loading concentration was 6 x 10^6 cells mL^{-1}, the percentage of empty droplets was minimal, but there was a high possibility (~90%) for the events of 4-10 cells per droplet (Fig. S3A, S3D). As the cell loading concentration was decreased to 6 × 10^5 cells mL^{-1}, 40 percent of the droplets successfully encapsulated 1-2 cells (Fig. S3B, S3E). When the cell loading concentration was further decreased to 6 × 10^4 cells mL^{-1}, nearly 80% of the droplets were empty (Fig. S3C, S3F). The rest of droplets encapsulated 1~3 cells for each. The frequency profiles of single-cell encapsulation by our method are comparable to the representative reports in the literature[42-44].

Development of the fluorescent assay to detect lactic acid.

In the reaction catalyzed by lactic dehydrogenase, lactic acid is oxidized into pyruvic acid, while nicotinamide adenine dinucleotide is converted into its reduced form (NADH) which becomes fluorescently detectable (Scheme 1B). Fluorescent measurements were performed to test different combinations of the reagents loaded in a 96-well microplate, including the control samples (1: Tris-HCl buffer; 2: LA in Tris-HCl; 3: NAD in Tris-HCl; 4: LDH in Tris-HCl; 5: NAD + LA in Tris-HCl; 6: NAD + LDH in Tris-HCl; 7: LA + LDH in Tris-HCl) and the positive sample (8: NAD + LA + LDH in Tris-HCl). As shown in Fig. 1A, the production of NADH by the reaction of LA and NAD in the presence of LDH enzyme made the positive sample solution (8) fluorescent, approximately a dozen folds more intensive than the control samples (1-7). The experiment verified that LA, NAD, and LDH were indispensable for this enzymatic reaction. The fluorescent signals by this assay were not interfered when the LA was replaced by different types of molecules such as glutathione, vitamin C, urea, glucose, arginine, and various inorganic ions including K^+, Na^+, Cu^{2+}, Mg^{2+}, Cl^-, which suggested an excellent specificity for this fluorescent assay (Fig. 1B). The excitation and emission spectra of the solutions in different combinations were acquired using a fluorescence spectrometer (HORIBA FluoroMax 4), verifying that utilization of the fluorescent property of the reaction product (NADH) allowed distinguishable measurements from the controls (Fig. 1C-D). The excitation peak (360 nm) and the emission peak (490 nm) were determined based on the spectral data. Optimization of the fluorescent assay was performed by titrating the concentrations of LDH and NAD separately. The fluorescence of the reaction was rapidly increased when the concentration of LDH was ranged from 0 to 500 U L^{-1}. Then we observed that the fluorescent increase was slowed down in the concentration of LDH from 50 U L-1 to 150 U L-1, followed by a typical plateau in the range from 150 U L^{-1} to 500 U L^{-1} suggesting a saturation of the fluorescence by the reaction (Fig. S4A). Fig. S4B presented a similar trend of the fluorescence changes correlating to the concentration of NAD, which indicated a saturation concentration of 6 mM for NAD. Therefore, the optimal concentrations were selected for LDH (200 U L^{-1}) or for NAD (6 mM). Since the reaction of generating NADH was accompanied with a change of H^+, the effect of changing the pH values on this reaction was investigated by fluorescence measurements, indicating the necessity of using the pH-stable buffer solution in the reaction for reproducible detection (Fig. S4C). We performed the time-course studies of the enzymatic reaction by monitoring the fluorescent changes of the mixture solutions (0-32 min) (Fig. S4D).

The solutions of lactic acid in a gradient concentration (including 25 µM, 50 µM, 75 µM, 100 µM, 250 µM, and 500 µM, respectively) were loaded in the microdroplets for the fluorescent measurements with our assay (Fig. 2A). Based on the standard curve, the limit of detection of our droplet-based assay was determined to be 1.02 µmol L^{-1} (S/N = 3) (Fig. 2B). In parallel, the performance of our fluorescent assay was compared against a commercial ELISA kit for the detection of lactic acid. As shown in Fig. 2C, the lactic acid solutions were loaded into a 96-well plate, and tested by the absorbance changes using the ELISA kit. A standard curve was established with the limit of detection of 67 µmol L^{-1} (S/N = 3) for the commercial kit. Therefore, our droplet assay can achieve the limit of detection nearly two orders of magnitude better than the commercial ELISA kit for quantitative analysis of lactic acid. Therefore, our droplet assay can achieve the limit of detection nearly two orders of magnitude better than the standard ELISA method of using a commercial kit for quantitative analysis of lactic acid. Noteworthy, our assay integrated a fluorescent detection method, while that commercial kit was based on the measurements of OD values assisted with an enzymatic amplification of the signals. The mechanistic difference between these two methods should also be considered in comparison of their performance.

Sensitive detection of lactic acid secreted by a single tumor cell.

Three different cell lines, including human adenocarcinoma alveolar basal epithelial cells (A549), human breast cancer (MCF7), human umbilical vein endothelial cell (HUVEC), were included in the tests of the droplet-based fluorescent assay for the detection of cell-secreted lactic acid. The fluorescent changes induced by cell-secreted lactic acid were measured using our droplet assay at 30 min, 60 min, and 90 min. The fluorescent images of the droplets and quantitative analysis for A549 cells are displayed in the main text (Fig. 3A), while the additional data for MCF7 and HUVEC cells are included in the supporting information (Fig. S5A and Fig. S6A). The fluorescence intensity of individual droplets was increased over the test time points, indicating that LA was secreted continuously by the cells. In the comparison of the two tumor cell lines (Fig. 3A and Fig. S5A), MCF-7 cells tended to secrete lactic acid slightly lower than A549 cells, which may be due to the variations in glycolytic process or the differential expression levels of the membrane

View Article Online
DOI: 10.1039/D0AY00637B

proteins (MCT1 and MCT4) for lactate transportation between these cell lines[21,45-48]. In contrast, the secretion of lactic acid by HUVEC cells was almost non-detectable under the normal culture condition (Fig. S6A). Furthermore, the chemical stimulation of the cells with a small molecular compound of PMA was tested with our droplet assay *in situ*. PMA can activate the phosphatidylinositol signaling pathway, thereby enhancing cell glycolysis to provide growth advantages both for normal cells and cancer cells[49]. Under PMA stimulation, all of these three different cell lines responded with the promoted secretion of lactic acid, exhibiting significant fluorescent increases in the microdroplets (Fig. 3B, Fig. S5B, and Fig. S6B). Based on the difference of the fluorescent signals (nearly 3 or 4 folds) between the cell lines, the tumor cells (A549 and MCF7) tended to have a higher glycolytic rates and proliferation than normal cells (HUVEC).

We attempted to calculate the amount of lactic acid secreted by a single cell based on the calibration curve using the droplet biosensor. Due to the effect of ultra-small volume (4.2 nL) confinement by the droplet, lactic acid molecules secreted by a single A549 cell can reach the detectable concentration quickly. As shown in Fig. 3C, the concentration of cell-secreted lactic acid accumulated inside the droplets was calibrated to be nearly 45 μM in the period of 30 min, and then gradually increased to 65 μM in the following incubation of 1 h. The analysis verified the positive enhancement on cellular secretion of lactic acid by the stimulation of PMA, consistent with our previous observation. We also performed quantitative calibration of the lactic acid concentration by a single MCF7 cell or HUVEC cell in the droplet with or without PMA stimulation, which provided the detailed profiles of cellular secretion in our tests (Fig. S5C, and Fig. S6C). In these experiments, multiple areas of interest (n=3) were randomly chosen for quantitative analysis of cellular secretion of lactic acid. Typically, there were approximately 60 droplets under the analysis for each testing condition. Based on our previous optimization, nearly 40% of the droplets encapsulated only a single cell, while the rest droplets could encapsulate either more than one cell or completely zero cell. The droplets of encapsulating zero cell were relatively easy to be distinguishable from the others. The case of encapsulating several cells simultaneously in one droplet was included into the data analysis in a limited tolerance. In parallel, the commercial kit for lactic acid detection was once more employed to measure the secretion levels of these different cell lines in the microplates. However, a large population of cells were required to be seeded into the wells of the microplate (2.4×10^5 Cells/well) for the signal readout, followed by a step to calculate the cell-secreted lactic acid on the average. The microplate results using the commercial kit suggested similar levels of lactic acid secretion (dozens of μM in hours), which verified the consistency of our single-cell droplet assay for cellular measurements (Fig. 3D, Fig. S5D, and Fig. S6D). Our droplet assay does not rely on large cell populations for signal readout. It allows for reliable quantification of lactic acid secretion by a single cell in a straightforward manner.

Glycolytic inhibitor screening with the single-cell droplet assay.

Anaerobic glycolytic metabolism is crucial to meet the energy requirements of cancer cells, with the by-product of lactic acid to modulate their microenvironment and gain growth advantages of decreased susceptibility to hypoxic stress[50]. Inhibition of the glycolytic pathway can deactivate the metabolic tricks and cut their energy supply, thus leading to cancer cell death particularly in hypoxic microenvironment. We tested our single-cell droplet assay on three small molecular inhibitors, including 3BP, VK_1, and VK_3, which targeted at a key rate-limiting enzymes in glycolysis pathway[41, 51, 52]. Among them, 3BP exhibited an intensive inhibiting effect on the cellular anaerobic glycolysis. As shown in Fig. 4A and Fig. S7A, it suppressed the fluorescence signals in the single-cell encapsulated droplets by dozens of folds in comparison to the untreated cells. In contrast, the tumor cells treated by VK_1 were mildly affected in their glycolysis pathway for lactic acid generation (Fig. 4B-C and Fig. S7B-C). The different inhibiting effects of these molecules by our droplet method was consistent to the reports in the literature[41, 51]. We performed the microplate experiments using the commercial kit to investigate the effects of the inhibitors on A549 cells and MCF7 cells. After the measurements of the absorption changes of individual wells (2.4×10^5 cells/well) induced by the inhibitors, we calculated the cellular lactic acid secretion on the average divided by the cell numbers (Fig. 4D and Fig. S7D). The results verified the difference between 3BP and VK_1 in glycolytic inhibition, as a positive indication of the feasibility of our droplet assay for the screening of glycolytic inhibitors.

In the experiments of cellular inhibition, the fluorescence changes of individual microdroplets were different from each other. As shown in Fig. 5A-B and Fig. S8A-B, occasionally a few microdroplets maintained their fluorescent intensity levels comparable to the untreated controls after incubation with the inhibitors (3BP or VK_3). We also observed a small percentage of microdroplets with relatively lower fluorescent signals, yet still not completely darkened in comparison to the droplets indicated by the white dash circles. 3BP is an inhibitor targeting at hexokinase and glyceraldehyde-3-phosphate dehydrogenase (GAPDH) in glycolysis. Given the fact of the high inhibiting efficiency of 3BP, the results as above suggested single cells individually out of the cell populations may find a way to survive from the unfavorable stress of glycolytic inhibition. VK_3 is an inhibitor targeting at the rate-limiting enzyme of pyruvate kinase, thereby slowing down the tumor glycolytic process[41]. Our experiments suggested that VK_3 was inferior to 3BP in the glycolytic inhibition. Therefore, we observed a moderate increase in the percentage of the A549-encapsulated microdroplets surviving the suppression of vitamin K3. Three independent experiments were performed for each condition to collect 300-600 microdroplets for statistical analysis (Fig. 5C-D and Fig. S8C-D). Importantly, we were able to acquire the profiles of lactic acid secretion of tumor cells under the influence of glycolysis inhibitors at the single-cell level. To the best of our knowledge, it presented the heterogeneous responses of individual tumor cells to glycolytic inhibitors for the first time. Although the assays based on the microplate format had been used for screening various inhibitors for cancer

research, they can only provide the results averaged on the cell populations, thus lack of the critical information why some cancer cells may escape from metabolic suppression induced by the specific inhibitors. Our droplet assay will offer a robust and useful tool to investigate cell-to-cell difference in glycolytic metabolism for the new advances in cancer therapies.

Conclusions

We report a new microfluidic assay to detect lactic acid secretion at the single cell level using droplets. Integration of the enzyme-assisted chemical reaction of lactic acid into the small volume droplets (4.2 nL) provides a straightforward and robust method for LA measurement by harvesting the intrinsic fluorescent signals of the reaction. We have demonstrated a sensitive and specific performance using the droplet assay. It allows us to investigate the effect of different chemical compounds including PMA and glycolytic inhibitors (such as 3BP, VK_1, VK_3) on the cellular secretion of lactic acid by a single tumor cell. It provides a tool to study abnormal cellular metabolism and reveal tumor cell heterogeneity in glycolytic pathways.

Conflicts of interest

There are no conflicts to declare.

Acknowledgements

This work is supported by the National Key Research and Development Program of China (2017YFE0131700), and by the National Natural Science Foundation of China (21874096, 21575095); a project supported by Collaborative Innovation Center of Suzhou Nano Science and Technology, joint International Research Laboratory of Carbon-Based Functional Materials and Devices, the 111 Project, and the Priority Academic Program Development of Jiangsu Higher Education Institutions (PAPD).

References

1 M. A. Swartz, N. Iida, E. W. Roberts, S. Sangaletti, M. H. Wong, F. E. Yull, L. M. Coussens and Y. A. DeClerck, *Cancer Res.*, 2012, **72**, 2473-2480.
2 D. F. Quail and J. A. Joyce, *Nat. Med.*, 2013, **19**, 1423-1437.
3 T. L. Whiteside, *Oncogene*, 2008, **27**, 5904-5912.
4 K. Nordfors, J. Haapasalo, M. Korja, A. Niemela, J. Laine, A. K. Parkkila, S. Pastorekova, J. Pastorek, A. Waheed, W. S. Sly, S. Parkkila and H. Haapasalo, *Bmc. Cancer*, 2010, **10**, 148.
5 C. T. Supuran, *Metabolites*, 2017, **7**, 48.
6 Y. Kato, S. Ozawa, C. Miyamoto, Y. Maehata, A. Suzuki, T. Maeda and Y. Baba, *Cancer Cell Int.*, 2013, **13**, 89.
7 K. Fischer, P. Hoffmann, S. Voelkl, N. Meidenbauer, J. Ammer, M. Edinger, E. Gottfried, S. Schwarz, G. Rothe, S. Hoves, K. Renner, B. Timischl, A. Mackensen, L. Kunz-Schughart, R. Andreesen, S. W. Krause and M. Kreutz, *Blood*, 2007, **109**, 3812-3819.
8 C. M. Cruciat, B. Ohkawara, S. P. Acebron, E. Karaulanov, C. Reinhard, D. Ingelfinger, M. Boutros and C. Niehrs, *Science*, 2010, **327**, 459-463.
9 C. T. Supuran, V. Alterio, A. Di Fiore, K. D' Ambrosio, F. Carta, S. M. Monti and G. De Simone, *Med. Res. Rev.*, 2018, **38**, 1799-1836.
10 F. Hirschhaeuser, U. G. A. Sattler and W. Mueller-Klieser, *Cancer Res.*, 2011, **71**, 6921-6925.
11 S. Blatt, N. Voelxen, K. Sagheb, A. M. Pabst, S. Walenta, T. Schroeder, W. Mueller-Klieser and T. Ziebart, *Clin. Oral. Invest*, 2016, **20**, 2097-2104.
12 M. Field, J. B. Block, R. Levin and D. P. Rall, *Am. J. Med.*, 1966, **40**, 528-547.
13 B. B. Lavietes, D. H. Regan and H. B. Demopoulos, *Proc. Natl. Acad. Sci. U.S.A.*, 1974, **71**, 3993-3997.
14 P. Sia, T. J. Plumb and J. A. Fillaus, *Am. J. Kidney Dis.*, 2013, **62**, 633-637.
15 S. Granja, I. Marchiq, R. Le Floch, C. S. Moura, F. Baltazar and J. Pouyssegur, *Oncotarget*, 2015, **6**, 6708-6721.
16 W. H. Koppenol, P. L. Bounds and C. V. Dang, *Nat. Rev. Cancer*, 2011, **11**, 325-337.
17 J. Fan, J. J. Kamphorst, R. Mathew, M. K. Chung, E. White, T. Shlomi and J. D. Rabinowitz, *Mol. Syst. Biol.*, 2013, **9**, 712.
18 C. Carmona-Fontaine, V. Bucci, L. Akkari, M. Deforet, J. A. Joyce and J. B. Xavier, *Proc. Natl. Acad. Sci. U.S.A.*, 2013, **110**, 19402-19407.
19 P. G. Haji-Michael, L. Ladriere, A. Sener, J. L. Vincent and W. J. Malaisse, *Metabolism*, 1999, **48**, 779-785.
20 F. Del Ben, M. Turetta, G. Celetti, A. Piruska, M. Bulfoni, D. Cesselli, W. T. S. Huck and G. Scoles, *Angew. Chem. Int. Ed.*, 2016, **55**, 8581-8584.
21 X. T. Zheng, H. B. Yang and C. M. Li, *Anal Chem*, 2010, **82**, 5082-5087.
22 P. Kumaresan, C. J. Yang, S. A. Cronier, R. G. Blazej and R. A. Mathies, *Anal Chem*, 2008, **80**, 3522-3529.
23 S. J. Spencer, M. V. Tamminen, S. P. Preheim, M. T. Guo, A. W. Briggs, I. L. Brito, D. A. Weitz, L. K. Pitkanen, F. Vigneault, M. P. J. Virta and E. J. Alm, *Isme. J.*, 2016, **10**, 427-436.
24 B. Tasic, *Curr. Opin. Neurobiol.*, 2018, **50**, 242-249.
25 S. Darmanis, S. A. Sloan, Y. Zhang, M. Enge, C. Caneda, L. M. Shuer, M. G. H. Gephart, B. A. Barres and S. R. Quake, *Proc. Natlc Acad. Sci. U.S.A.*, 2015, **112**, 7285-7290.
26 D. J. Chen, F. K. Fan, X. F. Zhao, F. Xu, P. Chen, J. Wang, L. Ban, Z. H. Liu, X. J. Feng, Y. H. Zhang and B. F. Liu, *Anal. Chem.*, 2016, **88**, 2466-2471.
27 Y. F. Liu, X. Y. Chen, Y. Q. Zhang and J. Liu, *Analyst*, 2019, **144**, 846-858.
28 A. B. Theberge, F. Courtois, Y. Schaerli, M. Fischlechner, C. Abell, F. Hollfelder and W. T. S. Huck, *Angew. Chem. Int. Ed.*, 2010, **49**, 5846-5868.
29 W. H. Fan, X. Chen, Y. Q. Ge, Y. Jin, Q. H. Jin and J. L. Zhao, *Biosens. Bioelectron.*, 2019, **145**,111730.
30 J. W. Choi, K. M. Min, S. Hengoju, G. J. Kim, S. I. Chang, A. J. deMello, J. Choo and H. Y. Kim, *Biosens. Bioelectron.*, 2016, **80**, 182-186.
31 M. Li, M. van Zee, C. T. Riche, B. Tofig, S. D. Gallaher, S. S. Merchant, R. Damoiseaux, K. Goda and D. Di Carlo, *Small*, 2018, **14**, 1803315.
32 Z. Yu, L. Zhou, T. Zhang, R. Shen, C. X. Li, X. Fang, G. Griffiths and J. Liu, *Acs Sensors*, 2017, **2**, 626-634.
33 R. Shen, P. P. Liu, Y. Q. Zhang, Z. Yu, X. Y. Chen, L. Zhou, B. Q. Nie, A. Zaczek, J. Chen and J. Liu, *Anal. Chem.*, 2018, **90**, 4478-4484.
34 34. J. Papaconstantinou and S. P. Colowick, *Fed Proc*, 1959, **18**, 298-298.
35 F. Gielen, R. Hours, S. Emond, M. Fischlechner, U. Schell and F. Hollfelder, *Proc. Natl. Acad. Sci. U.S.A.*, 2016, **113**, E7383-E7389.
36 Q. F. Xue and E. S. Yeung, *J. Chromatogr. A.*, 1994, **661**, 287-295.

View Article Online
DOI: 10.1039/D0AY00633E

37 C. Xintaropoulou, C. Ward, A. Wise, H. Marston, A. Turnbull and S. P. Langdon, *Oncotarget*, 2015, **6**, 25677-25695.
38 Y. L. Zhang, J. Y. Wei, J. Q. Xu, W. S. Leong, G. N. Liu, T. J. Ji, Z. Q. Cheng, J. Wang, J. Y. Lang, Y. Zhao, L. H. You, X. Zha, T. T. Wei, G. J. Anderson, S. Qi, J. Kong, G. J. Nie and S. P. Li, *Acs. Appl. Mater. Inter.*, 2018, **10**, 2347-2353.
39 E. Ehrke, C. Arend and R. Dringen, *J. Neurosci. Res.*, 2015, **93**, 1138-1146.
40 T. D. Wang and J. W. Kang, *Electrophoresis*, 2009, **30**, 1349-1354.
41 J. Chen, Z. Jiang, B. B. Wang, Y. G. Wang and X. Hu, *Cancer Lett.*, 2012, **316**, 204-210.
42 Y. C. Chao, S. Y. Mak, S. Rahman, S. P. Zhu and H. C. Shum, *Small*, 2018, **14**, 1802107.
43 S. Koster, F. E. Angile, H. Duan, J. J. Agresti, A. Wintner, C. Schmitz, A. C. Rowat, C. A. Merten, D. Pisignano, A. D. Griffiths and D. A. Weitz, *Lab Chip*, 2008, **8**, 1110-1115.
44 K. J. Son, D. S. Shin, T. Kwa, J. You, Y. D. Gao and A. Revzin, *Lab Chip*, 2015, **15**, 637-641.
45 A. Mongersun, I. Smeenk, G. Pratx, P. Asuri and P. Abbyad, *Anal. Chem.*, 2016, **88**, 3257-3263.
46 P. P. Liu, J. Liao, Z. J. Tang, W. J. Wu, J. Yang, Z. L. Zeng, Y. Hu, P. Wang, H. Q. Ju, R. H. Xu and P. Huang, *Cell Death Differ.*, 2014, **21**, 124-135.
47 M. G. Slomiany, G. D. Grass, A. D. Robertson, X. Y. Yang, B. L. Maria, C. Beeson and B. P. Toole, *Cancer Res.*, 2009, **69**, 1293-1301.
48 V. Ganapathy, M. Thangaraju and P. D. Prasad, *Pharmacol. Therapeut.*, 2009, **121**, 29-40.
49 W. F. Xu, F. Y. Zeng, S. Y. Li, G. H. Li, X. J. Lai, Q. J. Wang and F. Deng, *Cell Mol. Life Sci.*, 2018, **75**, 4583-4598.
50 G. L. Semenza, *Nat. Rev. Cancer*, 2003, **3**, 721-732.
51 L. S. Ihrlund, E. Hernlund, O. Khan and M. C. Shoshan, *Mol. Oncol.*, 2008, **2**, 94-101.
52 S. Ganapathy-Kanniappan, M. Vali, R. Kunjithapatham, M. Buijs, L. H. Syed, P. P. Rao, S. Ota, B. K. Kwak, R. Loffroy and J. F. Geschwind, *Curr. Pharm. Biotechno.*, 2010, **11**, 510-517.

View Article Online
DOI: 10.1039/D0AY00633E

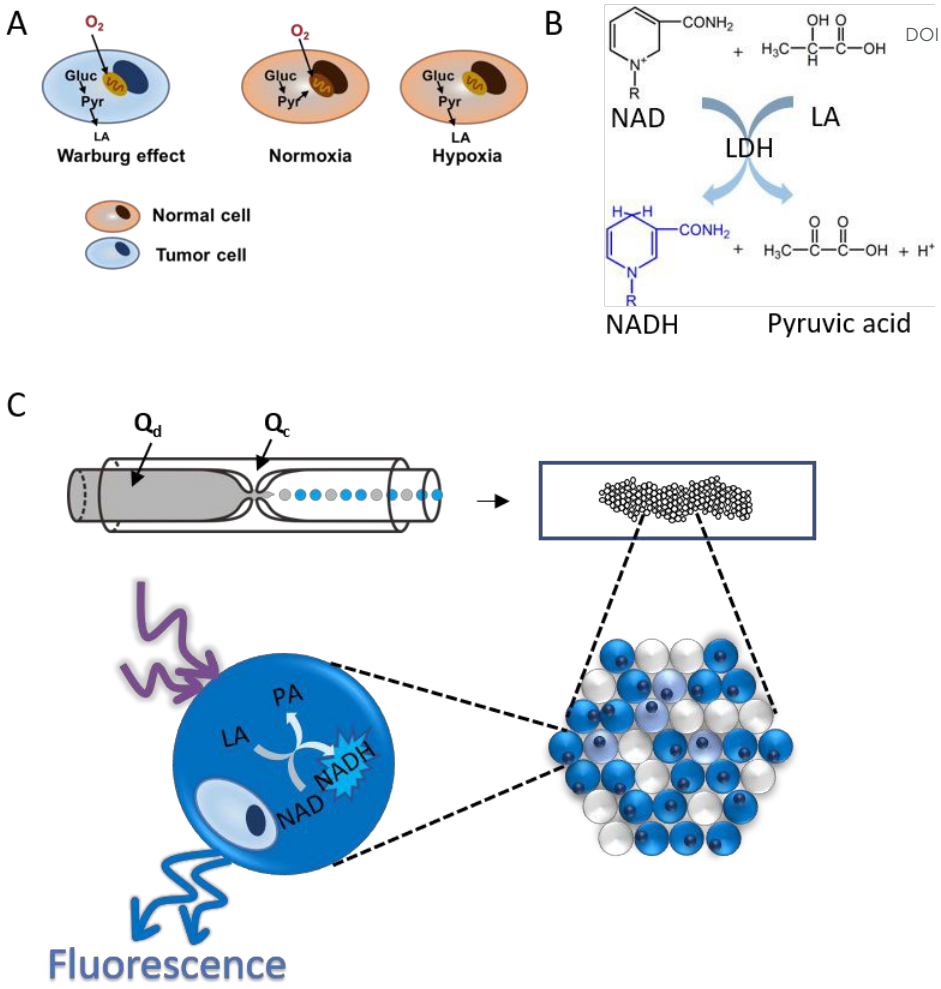

Scheme 1. (A) Schematic illustration of the Warburg effect in tumor cells for generation of lactic acid under normoxia, in comparison to the glucose metabolism in normal cells. (B) Assay principle: the chemical conversion of lactic acid to pyruvic acid assisted by lactic dehydrogenase, accompanied by the hydrogenation of nicotinamide adenine dinucleotide to generate the fluorescent by-product. (C) Sensitive detection of lactic acid secretion using single-cell encapsulated droplet biosensors.

View Article Online
DOI: 10.1039/D0AY00633E

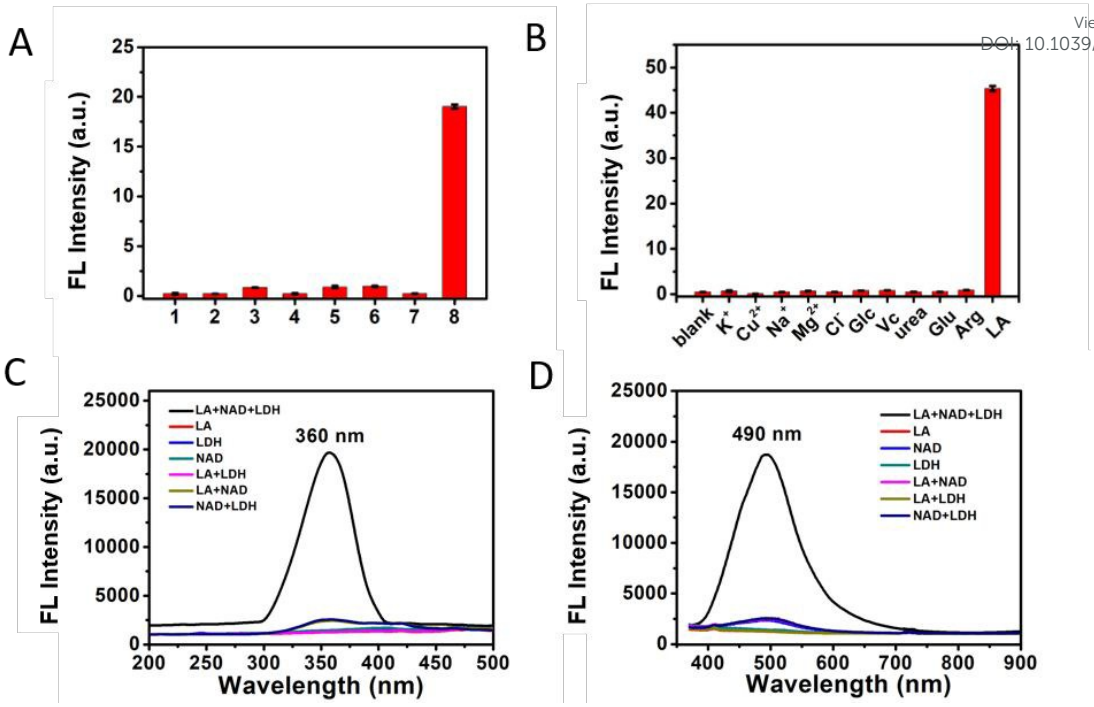

Fig. 1 Verification of the fluorescent assay for the detection of lactic acid. (A) Fluorescent measurements of the different combinations of the reagents with a microplate reader. Combination 1: the blank control; 2: LA; 3: NAD; 4: LDH; 5: NAD + LA; 6: NAD + LDH; 7: LA + LDH; 8: NAD + LA + LDH. All in the Tris-HCl buffer. (B) The specificity evaluation of the fluorescent assay using the ions and biomolecules (100 mM) as specified. (C-D) The excitation and the emission spectra of the reagent combinations as specified with a fluorescence spectrometer.

View Article Online
DOI: 10.1039/D0AY00633E

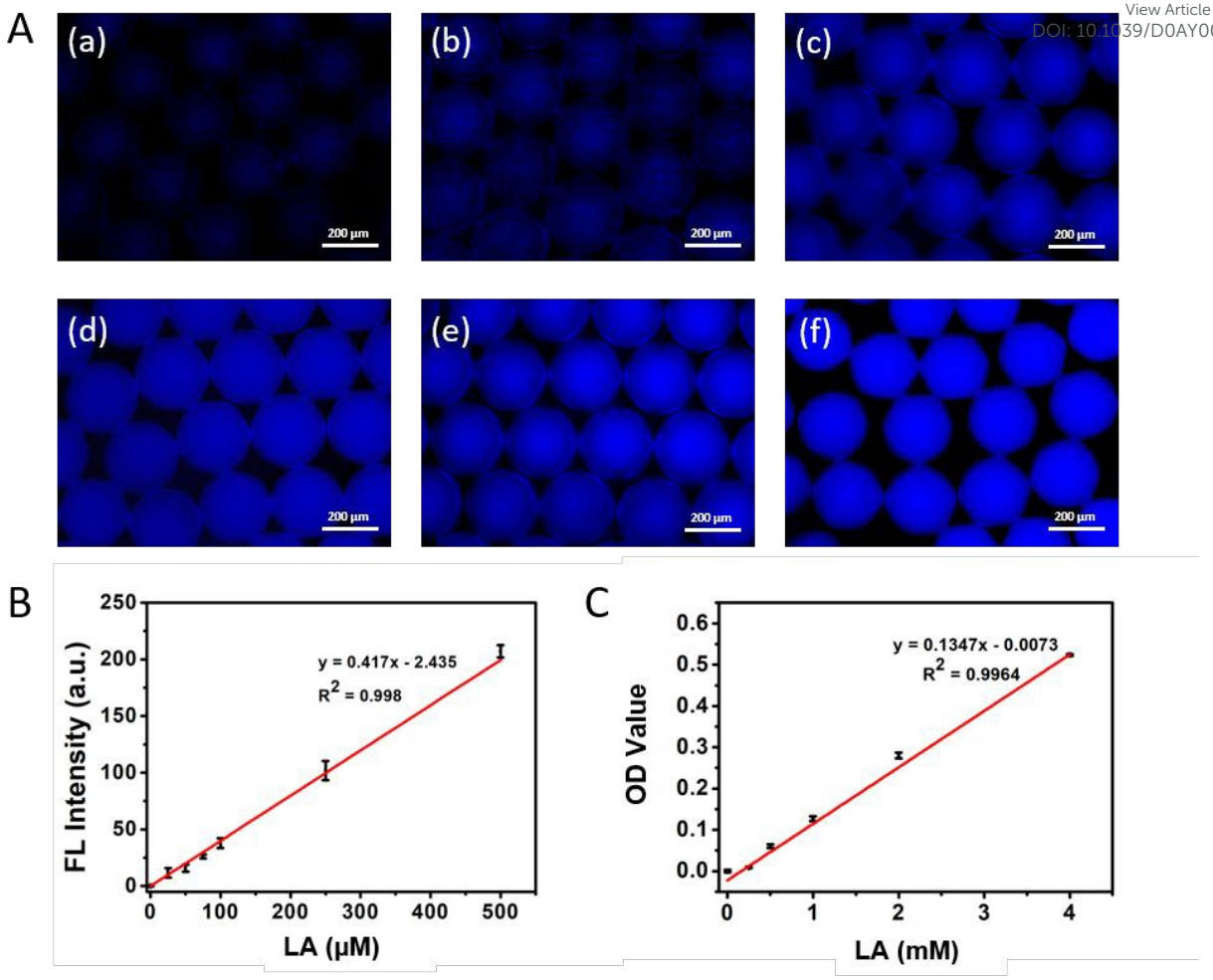

Fig. 2 Fluorescent measurements of the droplets in the titration of lactic acid concentrations. (A) Fluorescent images of the droplets containing lactic acid in gradient concentrations, including 25 μM, 50 μM, 75 μM, 100 μM, 250 μM, and 500 μM, respectively. Ex/Em: 360 nm/490 nm. (B) The standard curve of calibrating the fluorescence of the droplets and lactic acid concentrations. Error bars: standard deviation from different cubes (n=3). (C) The standard curve of calibrating the absorbance of the solutions and lactic acid concentrations in the microplate using the commercial kit. Error bars: standard deviation from different experiments (n=3).

View Article Online
DOI: 10.1039/D0AY00633E

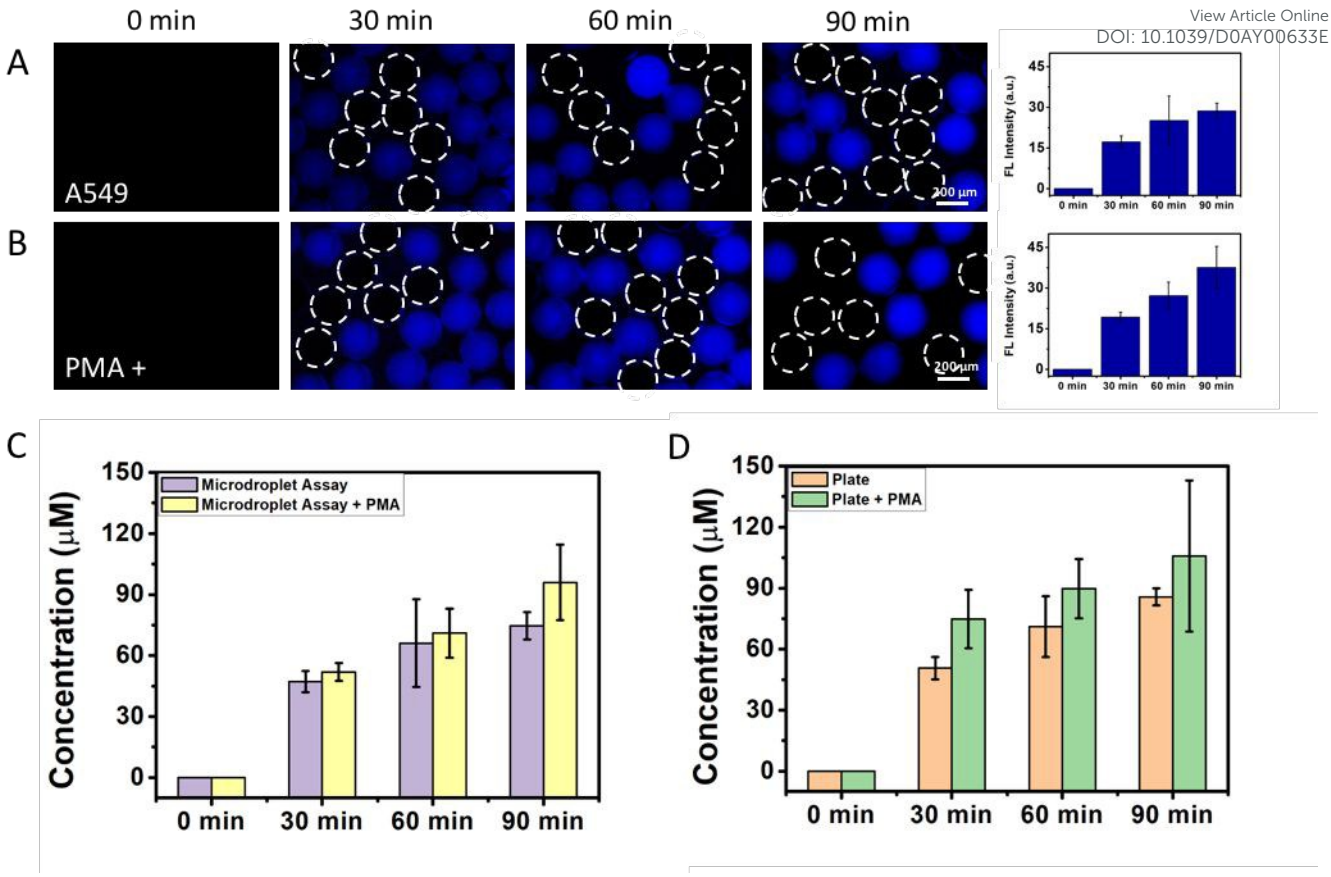

Fig. 3 Fluorescent measurement of droplets encapsulating single A549 cells at the time points of 0, 30, 60 and 90 min. (A-B) Fluorescent images and intensity analysis of A549 cells without or with PMA stimulation. Ex/Em: 360 nm/490 nm. The white circles: the empty microdroplets. Scale bar: 200 μm. Error bar: standard deviation from different cubes (n=3). (C) Lactic acid secretion of a single A549 cell using the droplet assay. Error bar: standard deviation from different cubes (n=3). (D) The averaged lactic acid concentrations secreted by A549 divided by the cell numbers in the microplate (2.4 $\times 10^5$ cells/well) using the commercial kit. Error bar: standard deviation from different experiments (n=3).

View Article Online
DOI: 10.1039/D0AY00633E

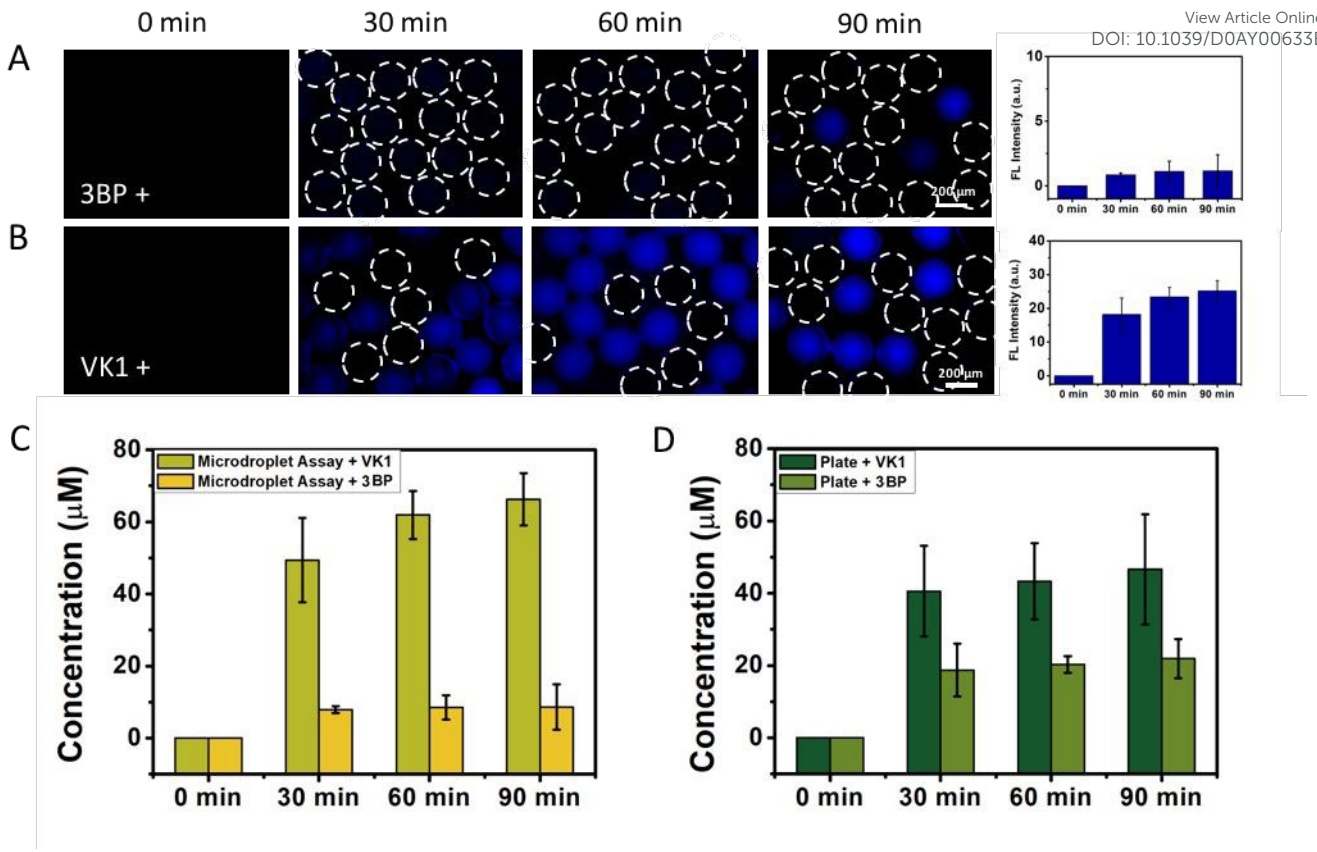

Fig. 4 Fluorescent measurement of droplets encapsulating single A549 cells at the different time points for glycolytic inhibitor screening. (A-B) Fluorescent images and intensity analysis of A549 cells with incubation of 3BP and VK_1. Ex/Em: 360 nm/490 nm. The white circles: the microdroplets with fluorescence below the threshold, either cellular LA scretion inhibited or no cell encapsulation. Scale bar: 200 μm. Error bar: standard deviation from different cubes (n=3). (C) Lactic acid secretion of a single A549 cell inhibitored by 3BP and VK_1 using the droplet assay. Error bar: standard deviation from different cubes (n=3). (D) The averaged lactic acid concentrations secreted by A549 divided by the cell numbers in the microplate (2.4×10^5 cells/well) using the commercial kit, under the inhibition of inhibitored by 3BP and VK_1. Error bar: standard deviation from different experiments (n=3).

View Article Online
DOI: 10.1039/D0AY00633E

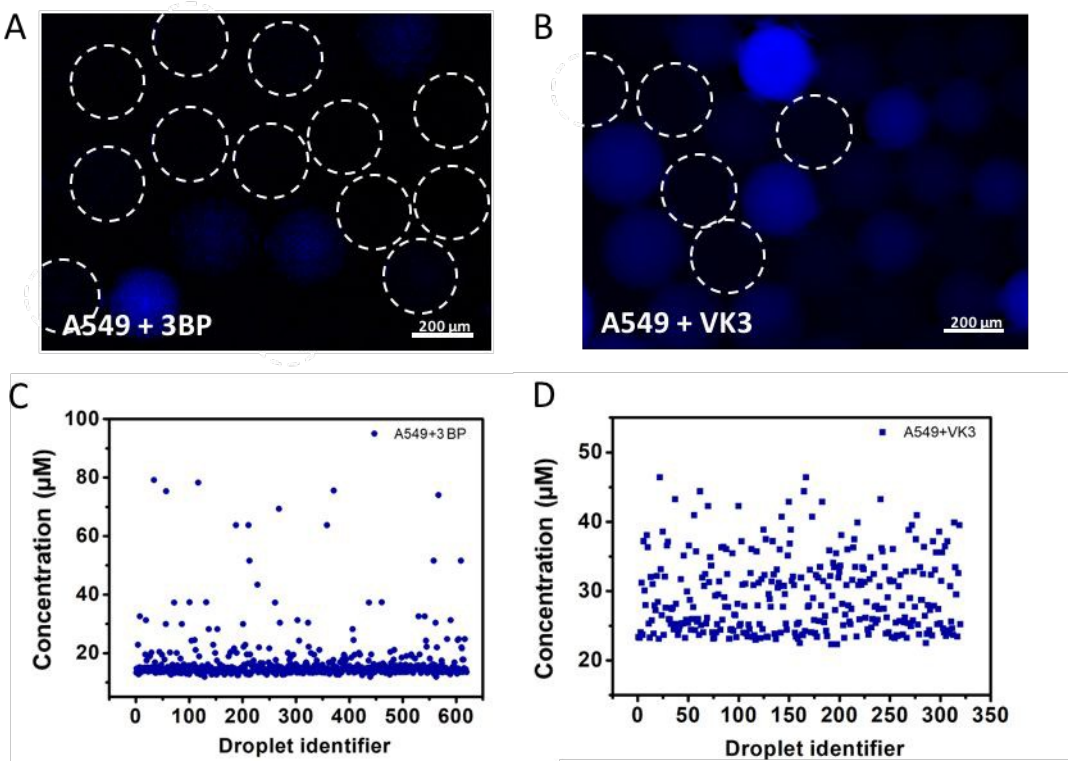

Fig. 5 Lactic acid secretion of A549 inhibited by 3BP to VK_3 using the droplet assay, suggesting cell-to-cell difference in glycolytic processing. (A-B) Fluorescent images of A549 cell-encapsulated droplets with incubation of 3BP or VK_3. Ex/Em: 360 nm/490 nm. The white circles: the microdroplets with fluorescence below the threshold, either cellular LA scretion inhibited or no cell encapsulation. Scale bar: 200 μm. Error bar: standard deviation from different cubes (n=12, n=6). (C-D) Scatter plots of single-cell secreted lactic acid concentration in the individual droplets.

View Article Online
DOI: 10.1039/D0AY00633E